ELSEVIER

Journal of Chromatography A, 979 (2002) 33–42

JOURNAL OF CHROMATOGRAPHY A

www.elsevier.com/locate/chroma

Sub-second liquid chromatographic separations by means of shear-driven chromatography

D. Clicq[a,*], N. Vervoort[a], R. Vounckx[b], H. Ottevaere[c], J. Buijs[d], C. Gooijer[d], F. Ariese[d], G.V. Baron[a], G. Desmet[a]

[a]*Department of Chemical Engineering, Vrije Universiteit Brussel, Pleinlaan 2, 1050 Brussels, Belgium*
[b]*Department of Electronics, Vrije Universiteit Brussel, Pleinlaan 2, 1050 Brussels, Belgium*
[c]*Department of Applied Physics & Photonics, Vrije Universiteit Brussel, Pleinlaan 2, 1050 Brussels, Belgium*
[d]*Department of Analytical Chemistry and Applied Spectroscopy, Vrije Universiteit Amsterdam, De Boelelaan 1105, 1081 HV Amsterdam, The Netherlands*

Abstract

Utilizing the concept of shear-driven chromatography, we have been able to realize reversed-phase LC separations in flat rectangular nano-channels coated with a C_8 monolayer and being as thin as 100 nm. At this scale, the separation kinetics are strongly enhanced, as is witnessed by the extremely short time (<0.1 s) needed to separate a mixture of coumarin dyes. The observed plate numbers are still relatively small, because the experiments were conducted in ultra-short columns (≤1 mm) and under injection band width-limiting conditions.

Keywords: Shear-driven chromatography; Instrumentation; Injection bands; Coumarins; Dyes

1. Introduction

In the past decades, large experimental efforts have been devoted to increase the velocity of LC separations. With the advent of the so-called laboratory on-a-chip approach [1–3], allowing one to pursue the kinetic advantages of miniaturized flow and separation systems, and with the ever growing demand for increased separation capacity coming from the field of pharmaceutical research and clinical diagnostics, the interest in rapid separations has even further increased. By switching to electrically driven systems, groundbreaking work in the field of rapid analysis has, amongst others, been presented by Moore and Jorgenson [4], Jacobson et al. [5] and Kütter et al. [6]. Demonstrations of the generation of over 1 000 000 theoretical plates in less then 46 s [7], the separation of five polycyclic aromatic hydrocarbons in less than 5 s [8], and even sub-millisecond separations of Rhodamin B and dichlorofluorescein [9] have been reported as well.

In a novel approach, aiming at the omission of the problems related to the lack of robustness and the fluid composition dependence of the migration times in capillary electrochromatography (CEC) [10], we have recently proposed [11] the technique of shear-driven flow chromatography (SDC). This novel approach is based on the use of an axially split channel system, consisting out of two highly polished flat surfaces, into one of which a half-open

*Corresponding author. Tel.: +32-2-629-3617; fax: +32-2-629-3248.
E-mail address: david.clicq@vub.ac.be (D. Clicq).

0021-9673/02/$ – see front matter
PII: S0021-9673(02)01264-5

channel is recessed. By axially moving one part past the other, a flow system is obtained wherein the fluid velocity is mechanically imposed along each point of the channel length [12]. As a consequence, the established flow-rates are perfectly predictable and reproducible and do not depend upon a sensitive parameter such as the channel wall zeta-potential, as is the case in electrically driven systems. Furthermore, as the SDC concept is devoid of any pressure of voltage gradient limitation, and as there are no problems of double-layer overlap, it opens the road towards a new range of enhanced separation kinetics: as it allows to use channels with a sub-micron thickness (which is highly advantageous because the speed of chromatographic separation is known to scale according to d^{-2} [13]) without any limitation on the applicable fluid velocity, it has the potential to break the 100 000 plates/s limit [11]. The major hurdle on the road to the realization of the full separation potential of SDC is, however, the required degree of miniaturization of the injection and detection facilities. The need to inject and detect minute sample amounts in a reproducible and sufficiently sensitive way is a problem which is common to all miniaturized separation techniques, but with the envisioned extreme dimensions of the SDC channels, the problem is of course more critical. The SDC system, however, also displays a number of unique features which can be exploited to facilitate and enhance the injection and detection [14]: the open-channel format enabling the application of novel stationary phase micromachining techniques, the sub-micron channel thickness enabling the incorporation of a transversally running light pipe for UV–Vis absorption detection.

In a series of progressively demanding experiments, we are now working on the demonstration of the practical feasibility of the SDC concept. First a series of nano-channel tracer flow experiments has been conducted [12], showing that the established fluid velocity in SDC always exactly equals one-half of the imposed moving wall velocity, independently of the viscosity, the pH and the conductivity of the liquid, and showing that the use of axially split channels does not create any undesired side-ways leakages. In a next step, we have realized a series of preliminary separations of Methylene Blue/Rhodamin B colour tracers in printed channels with a thickness of 4 μm, confirming that LC type separations can indeed be effectuated without an externally imposed flow driving gradient [15]. In the present contribution, we report on the recent progress we made. Due to a switch to more advanced detection technology, we have now been able to downscale the thickness of our separation channels to the ultimately pursued 100-nm level. Using an air-cooled fluorescence CCD camera and injecting strongly fluorescing coumarin dyes, real-time images of nano-channel separations could be made.

2. Experimental

2.1. Apparatus and experimental set-up

A schematic view of the used experimental set-up is shown in Fig. 1. The heart of the set-up is an upright epi-fluorescence microscope (Nikon Microphot-FXA, Cetec, Belgium), equipped with a UV-1 filter cube set (UV-2A, MBE-14100, Cetec), with excitation at 350 nm and emission above 450 nm, allowing to use the light of a Hg-vapor lamp (Nikon HB 101-AF, Cetec) to excite the coumarin dyes of the test samples in the UV and to detect the emitted fluorescent light around 460 nm. The (movable) bottom part of the SDC channels is attached to the microscope table by putting it in a stainless steel

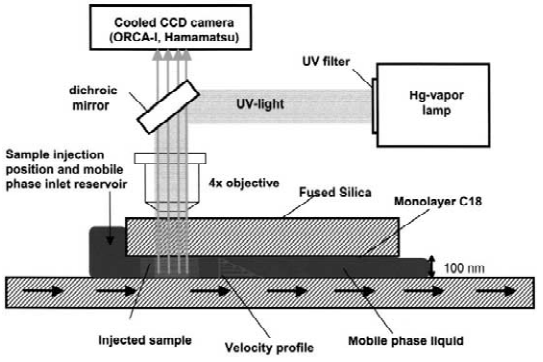

Fig. 1. Schematic drawing (not to scale) of the experimental set-up (motorized linear displacement system used to translate the microscope table is not represented).

fixation frame mounted on top of the microscope table. The (stationary) top part of the SDC channels is then positioned underneath the objective lens (×4 magnification and UV transparent, Nikon CE Plan Achromat, Cetec) using an in-house made attachment piece already described previously [14]. With this approach, the set-up is kept very compact and the position of the channel can be controlled very precisely.

The separations were visualized using an air-cooled CCD fluorescence camera (ORCA-ER C4742-95, Hamamatsu Photonics, Belgium) mounted on the video adapter of the microscope. The camera could be operated at a frame rate of 53 Hz when operated in the 8×8 binning mode. The video frames were digitally captured using a Matrox-Meteor2-Dig card (Hamamatsu Photonics). The video images were subsequently analyzed with the accompanying Simple-PCI 4.0 software.

The microscope was mounted on a breadboard (M-IG 23-2, Newport, The Netherlands), together with a linear displacement stage (M-TS100DC.5, Newport) equipped with a stepping motor (UE611CC, Newport) and a speed controller (MM, 4006 Newport). This system offers a positioning accuracy of 0.5 μm and provides a displacement velocity range going from 1 μm/s up to 10 cm/s. Using another in-house made connection piece, the motorized displacement stage was used to automatically translate the microscope table, both during the injection procedure (see Section 2.3) and the subsequent separation runs.

Prior to each series of runs, it was ensured that the stationary and moving channel part were in perfect contact, by verifying that no fluorescence light is emitted from the surface parts adjacent to the recessed channel. At this position, both channel parts normally should be in intimate contact. When the sample liquid spreads outside the recessed channel opening, this is an indication of the fact that the channel parts are not well positioned (e.g., because of the presence of a dust particle). This also implies that the thickness of the fluid layer in the channel is much larger than the nominal depth of the channel. This of course leads to undesired peak broadening. When such a mismatch of the channel parts was noted, both parts were removed and thoroughly cleaned with pure methanol.

2.2. Channel manufacturing

The half-open nano-channels needed for the stationary wall part of the SDC channels were obtained by reactive ion etching using a CHF_3-plasma in a Plasma-therm Batchtop IV-oven (TPS, UK). The channels were recessed in flat polished fused-silica substrates (Plan Plate 390116, Linos Photonics, The Netherlands) and always ran across the entire length ($L=15$ mm) of the stationary wall substrates. They were typically 4 mm wide. Channels with different etch depths, all ranging between 100 and 1000 nm, were prepared. The exact depth of the channels was investigated using a WYKO depth-profiling system (Veeco Instruments, UK). With this laser-interferrometry based measurement system, large parts of the surface (scan field=0.91×1.2 mm) can be inspected in a single step with a spatial resolution of about 12 μm^2 (368×238 pixels for the 0.91×1.2-mm scan field) and with a depth resolution around 1 nm. As the apparatus furthermore enables stitching mode measurements, highly accurate depth profile scans of the entire channel can be made. For the moving wall part of the SDC channels, another flatly polished fused-silica glass plate (Plan Plate 390118, Linos Photonics) was used. This plate had a flatness of $\lambda/20$ ($\lambda=512$ nm), and was substantially larger (i.e., 5 cm) than the stationary wall plate. The latter is needed to ensure a sufficient travel length.

For the derivatization of the channel walls, a protocol similar to the one described in Ref. [16] has been used. Briefly, the fused-silica plates were first sequentially rinsed with 1 *M* potassium hydroxide, 0.03 *M* hydrochloric acid, purified water and HPLC-grade methanol (cas no. 67-56-1, Fluka, Belgium) for 30 s each. The plates were then dried overnight at 110 °C. Subsequently, the fused-silica plates were put into a 10% (w/w) solution of chloro-dimethyloctylsilane (cas no. 14799-93-0, Sigma–Aldrich, Belgium) in toluene for 24 h at room temperature. Afterwards, the silica plates were sequentially washed with toluene and methanol, and dried with purified air.

2.3. Injection mode, and sample and mobile phase composition

The test samples were prepared by mixing and

dissolving two different coumarin dyes (coumarin C440, cas no. 26093-31-2; and coumarin C460, cas no. 91-44-1, both purchased from Across Organics, Geel, Belgium) into different water–methanol solutions with variable volume ratio. In all the separation experiments, the coumarins C440 and C460 were injected at a concentration of 1.5×10^{-3} *M* each, in order to have a sufficient S/N ratio. Working in the 8×8 binning mode, and carefully selecting the right focal plane, the detection limit for the coumarins was found to be of the order of 1×10^{-4} *M*. The mobile phase was prepared by mixing the appropriate percentage of HPLC-grade methanol in purified water (Nanopure II, Barnstead, Van Der Heyden, Belgium).

Narrow sample plugs (order 100 μm) were injected using a dedicated injection procedure already described previously [14]. Briefly, the procedure occurs in four successive steps. In the first step, the mobile phase present in the reservoir in front of the channel is removed by aspirating it away using a flexible tube with a modified pipette-tip mounted on its top and connected to a vacuum pump (Adeb 63, AEG, Belgium). This first step currently occurs manually and has no strict time limitation. In the second step, sample is loaded in front of the channel inlet (see arrow indication in Fig. 1) using a standard micropipette. During the third step, the moving wall is displaced rapidly ($u_{wall}=10$ mm/s) over a given prescribed distance. To inject a 100-μm band, the wall has to be displaced over exactly 200 μm, because the liquid inside the channel is known to flow at exactly one-half of the moving wall velocity [12,14]. During the fourth and final step, the motion of the moving wall is briefly interrupted to aspirate away the non-entered sample and to replace it by fresh mobile phase liquid. To avoid excessive injection band broadening due to the inevitable inward diffusion effects taking place during steps 2–4, these steps have to be kept as short as possible. Currently, these steps are effectuated in a time frame of about 4–6 s, but obviously this has to be reduced to minimize the contribution of the undesired diffusive flux to the total injection flux [14].

All the experiments were performed at ambient temperature ($T\cong20$ °C). The imposed mobile phase velocity during the separation runs was varied between 1 mm/s and 1 cm/s. The range of velocities larger than 2 cm/s is currently inaccessible because of the limited capture rate of our CCD detection system.

3. Experimental results

3.1. Channel manufacturing

Fig. 2 shows a cross-sectional WYKO scan of one of the reactive ion etched SDC channels used in the present study. The channel cross-section clearly displays the desired rectangular shape. The reader should also note the extreme aspect ratio: the *x*-scale is in millimeters, whereas the *y*-scale is in nanometers. The average depth of the channel is about 120 nm. The maximal average depth variation over the entire channel length of 15 mm typically is about 10 nm. The surface roughness of the fused-silica substrates is clearly increased by the etching process, as can be noted from the fact that the surface in the recessed parts displays a much larger roughness than the non-etched higher parts. The increased roughness is probably due to the presence of impurities in the fused-silica glass. Future work will be conducted to investigate this more closely.

3.2. Injection and tracer flow experiments

Fig. 3 shows a series of video frame images of different injected tracer bands. The frames were taken at about the same position in the channel (i.e., about 200 μm downstream of the channel inlet). In these experiments, the coumarin C460 was injected at a concentration of 10^{-2} *M*, in order to have a

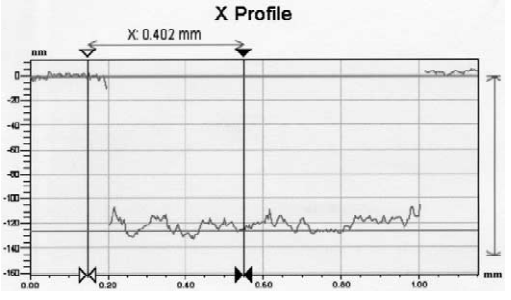

Fig. 2. Wyko-scan measurement of the cross-section of one of the RIE etched nano-channels employed in the current study.

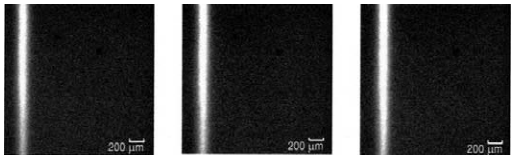

Fig. 3. Still CCD camera images of three different injections performed in the 100-nm channel. Each image corresponds to the first video frame ($t=0.018$ s) obtained after retaking the translation of the moving wall.

better S/N ratio of the images. As can be noted, the reproducibility of the injections is very good.

3.3. Separation experiments

Fig. 4 shows a series of selected video frames of a rapid separation of a coumarin C440/C460-mixture in a channel with nominal depth $d=410$ nm, using a mobile phase composition of methanol–water (23:77, v/v) and for a mobile phase velocity of 10 mm/s. In an overlay plot, we show the pixel intensity values as obtained from the Simple PCI-image analysis software, and averaged over the y-direction. The latter was found to be absolutely indispensable for the achievement of a sufficient S/N ratio. The corresponding frame times are given as well, showing that the two coumarins are clearly base-line separated within a time span of about 0.06 s. Injection of the individual components revealed that the most rightward peak (i.e., the least retained peak) was the coumarin C440, in agreement with the reversed-phase CEC measurements presented in Refs. [5,6].

Fig. 5 shows the most rapid separation performed in a channel with nominal depth $d=120$ nm. To increase the speed of the peaks to the level of that in the $d=410$ nm channel, we raised the concentration of the organic component of the mobile phase to a value of 32%.

Fig. 6 shows the adopted procedure for the calculation of the retention factor and the theoretical plate height values used to interpret the SDC separation experiments. From the individual video frames, the retention factor k of the sample com-

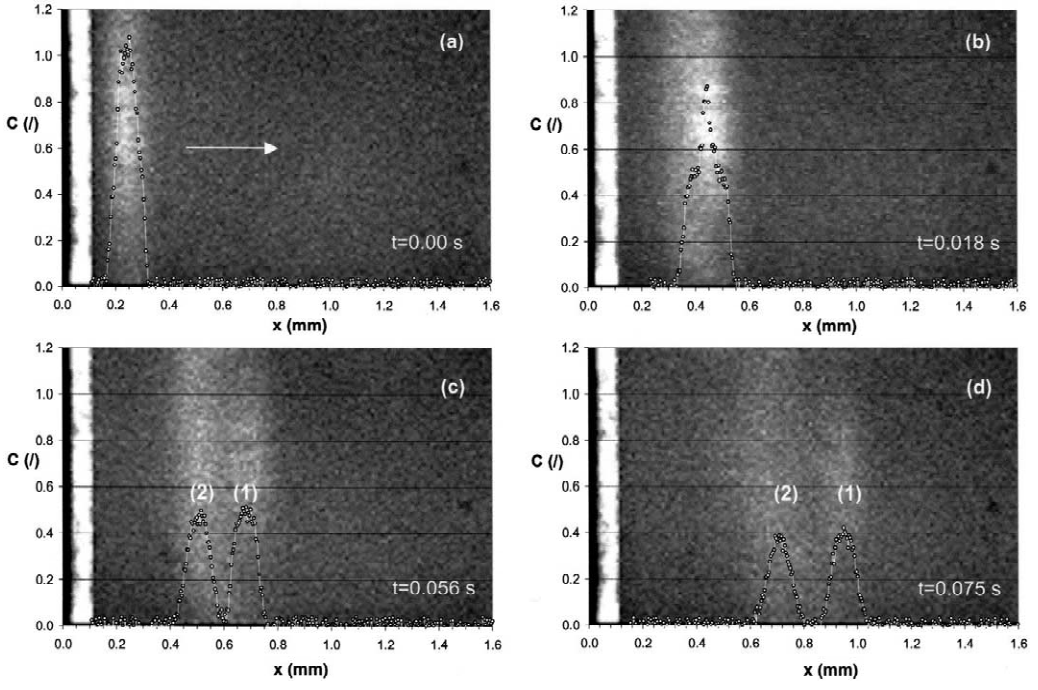

Fig. 4. Sequence of four successive video frames images and overlaid corresponding intensity plot of a separation of coumarin C440 and C460 performed in the $d=410$ nm (1) channel C440, (2) C460, $u=10$ mm/s, injected sample $=1.5\times10^{-3}$ M C440 and 1.5×10^{-3} M C460; mobile phase, methanol–water (32:68, v/v). The white arrow in (a) indicates the direction of the mobile phase flow.

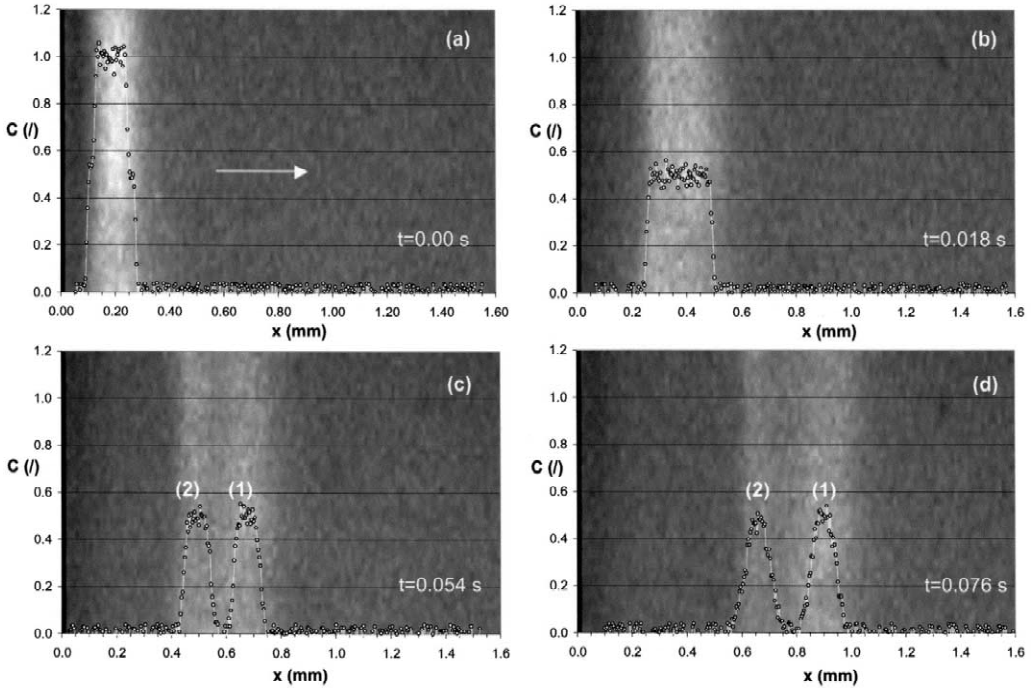

Fig. 5. Sequence of four successive video frames images and overlaid corresponding intensity plot of a separation of coumarin C440 and C460 performed in the $d=120$ nm channel. (1) C440, (2) C460, $u=10$ mm/s, injected sample $=1.5\times10^{-3}$ M C440 and 1.5×10^{-3} M C460; mobile phase, methanol–water (33:77, v/v). The white arrow in (a) indicates the direction of the mobile phase flow.

ponents could be derived from the difference between the position L_0 of a virtual line representing the velocity of the non-retained mobile phase liquid (moving with exactly one-half of the moving wall velocity, see Ref. [12]), and the actual position L_{eff} of the moving dye peak, using:

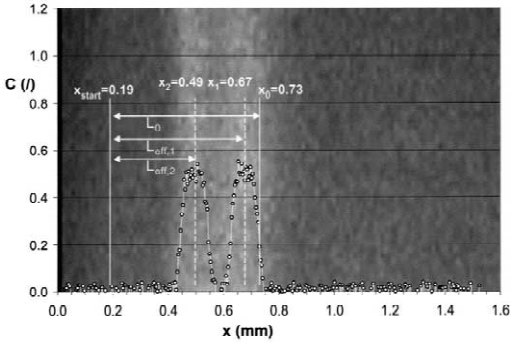

Fig. 6. Elaboration of the graphical procedure adopted to calculate the peak retention factors.

$$k=\frac{L_0-L_{\text{eff}}}{L_{\text{eff}}} \tag{1}$$

From the peaks in the colour intensity plots, estimates of the theoretical plate height could be made, using the variance σ_x^2 of the peak, using:

$$H_{\text{exp}}=\frac{\sigma_x^2}{L_{\text{eff}}} \tag{2}$$

The σ_x^2 values were determined from the widths of the peaks in the intensity plots. For the situation in Fig. 6, the above analysis yields a value of $k_1=0.11$ (±0.02) and $H_{\text{exp},1}=1.3$ μm (±0.1 μm) for the first peak and $k_2=0.44$ (±0.03) and $H_{\text{exp2}}=2.2$ μm (±0.1 μm) for the second peak. The first peak yields a plate number of about $n=370$, the second peak yields about $n=190$. It should be recalled that these data have been calculated using Eq. (2), implying that they are strongly influenced by the injection band width (see Section 4).

In principle, these H_{exp} values can be corrected by subtracting the variance $\sigma^2_{x,inj}$ of the injected peak using:

$$H_{exp,corr} = \frac{\sigma_x^2 - \sigma_{x,inj}^2}{L_{eff}} \quad (3)$$

The thus obtained values were however found to be too error sensitive to be used for a statistically relevant data analysis.

A summary of the H_{exp} data for two series of separation runs, one conducted in the $d = 410$ nm channel, one in the $d = 120$ nm channel, is given in Fig. 7. All data were evaluated from a video frame wherein the first peak was near the $x = 1$ mm position. Although only the H_{exp} values for the second peak are given, it should be noted that the H_{exp} values for the first peak relate in a fully similar manner to the theoretical expectations. Each experiment was performed twice. The error bars give the lowest and smallest value of the experiments. Comparing the $d = 410$ nm data to those for the $d = 120$ nm channel, no really significant difference can be observed. This is for a large part due to the fact that the presently presented experiments are conducted in the injection band width-limited regime (see also Section 4). The average k values for the experiments conducted in the 120-nm channel and for a mobile phase composition of methanol–water (32:68, v/v) were, respectively, found to be given by $k_1 = 0.09$ (standard deviation = 0.02), and $k_2 = 0.54$ (standard deviation = 0.04). For the experiments conducted in the 410-nm channel and for a mobile phase composition of methanol–water (23:77, v/v), the retention factors were, respectively, found to be $k_1 = 0.11$ (standard deviation = 0.02) for the first peak, and $k_2 = 0.48$ (standard deviation = 0.03) for the second peak.

4. Discussion

As is well-known from the field of ultra-rapid CE, it is critical to accurately inject narrow tracer bands (axial width of the order of 100 μm or less) [17,18]. Even with the highly efficient injection devices developed for on-chip CE, the achievable plate number of rapid separations occurring over very short channel lengths is nearly completely determined by the injection band width [6,18]. With the semi-automated injection procedure, and due to the high displacement accuracy of the employed translation stage, we are now able to very reproducibly inject tracer bands of the order of 100 μm. This is clearly evidenced by the sequence of injection experiments presented in Fig. 3. Making a statistical analysis of the conducted injection experiments, we can state that the motorized translation stage now allows to inject narrow bands of the order of 100 μm with a standard deviation of about 10%. As was outlined in a more in-depth study of the currently employed injection process [14], the major contribution to this variance originates from the variable timing of steps 2–4 of the injection process (cf.

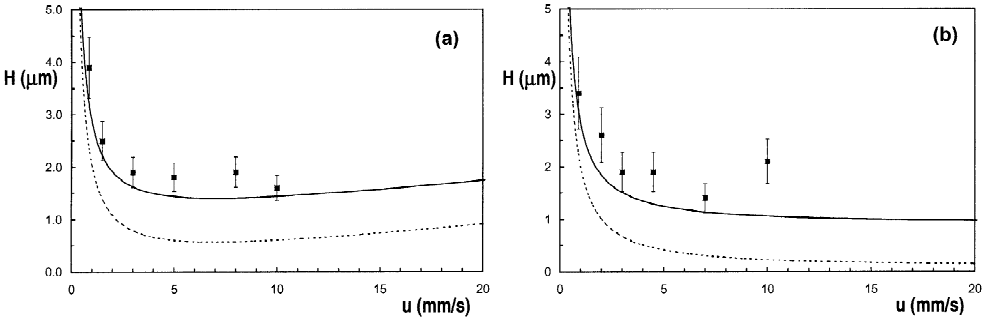

Fig. 7. Comparison between the experimental theoretical plate height values and the theoretical expectation (dashed lines = $H_{col,theo}$ values calculated from Eq. 4, full lines = $H_{tot,theo}$ values calculated from Eq. 5) for the second peak (C460) in the chromatograms. (a) H_{exp} values for the $d = 410$ nm channel (data used for theoretical curves: $d = 410$ nm, $D_{mol} = 5 \times 10^{-10}$ m^2/s, $w = 100$ μm, $k = 0.48$) and (b) H_{exp} values for the $d = 120$ nm channel (data used for theoretical curves: $d = 120$ nm, $D_{mol} = 5 \times 10^{-10}$ m^2/s, $w = 100$ μm, $k = 0.54$).

Section 2.3). These are still effectuated manually and take about 4–6 s. During this time, a significant diffusive inward leakage occurs. With a fully automated injection system, capable of reducing the injection step duration to about 0.5 s, it should be possible to reduce the injection band width variation to below 1% [14]. Considering that the employed translation stage has a displacement resolution of 0.5 μm, it should be obvious that the injection of more narrow sample bands (of the order of 50 μm or even smaller) is perfectly feasible. However, the contribution of the diffusive leakage becomes much more pronounced in this case, and, furthermore, the detectability of the peaks also strongly diminishes. It therefore turns out that 100-μm injections currently yield the best compromise between reproducibility and detectablity on the one hand, and resulting separation resolution on the other hand.

With the microscope set-up we are limited to CCD recordings of the first 1.6 mm of the channel. We therefore selected the chromatographic conditions such that the peaks became base-line separated in this first section. With the disposition of a system with extremely short radial diffusional distance, the current set-up is hence especially suited to explore the separation speed limits of LC.

Figs. 4–5 clearly demonstrate that the coumarin C440–C460 mixture can easily be separated in less than 0.1 s. Using only a monolayer C_8 coating, without the application of any specific roughening treatment to increase the specific surface of the stationary channel wall, the channels nevertheless clearly yields sufficient retention capacity to separate the coumarins in a very short distance. This is due to the unusually small channel thickness, greatly increasing the phase ratio over other mono-layer coated open-tubular channel systems with a diameter of the order of for example 5–10 μm. The base-line separation time of less than 0.1s is about two orders of magnitude smaller than in the coumarin separation chromatograms presented by Kutter et al. [6]. To the best of our knowledge, they have reported the fastest coumarin separation achieved thus far. They performed microchip open-channel electrochromatography in channels with different depths varying between 10.2 and 2.9 μm. The analysis times which can be estimated from their chromatograms are of the order of 10–20 s, although the conditions of the separation and the achieved efficiencies are clearly different from ours, hence it is difficult to do a correct comparison. The presently proposed sub-0.1-s separations however clearly reflect the rapid separations kinetics of the SDC system. As already mentioned, these enhanced separation kinetics stem from two different advantages: (i) the possibility to apply mobile phase velocities significantly larger than those in electrically driven and pressure-driven systems, and (ii) the possibility to use nanometric thin channels without the complication of double-layer overlap and without any limitation on the applicable mobile phase velocity. Due to the very short radial dimensions, nanometric thin channels yield extremely short radial diffusion times (of the order of 10^{-5} s for a solute with $D_{\mathrm{mol}} = 10^{-9}$ m^2/s in a channel with $d = 100$ nm, as can be calculated from Einstein's diffusion law [19]). The mobile phase mass transfer resistance then reduces correspondingly.

Considering the achieved separation efficiencies, it has to be noted that they are still far away from the theoretical expectations. The major reason for this deviation has to be found in the large contribution of the injection band width. As demonstrated earlier [11], the theoretical plate height of an SDC system with flat rectangular cross-section and with a negligible stationary phase contribution (corresponding to the fact that we only employed monolayer stationary phase coatings in the SDC channels) is given by:

$$H_{\mathrm{col,theo}} = 2\frac{D_{\mathrm{m}}}{u} + \frac{2}{30}\cdot\frac{1+7k+16k^2}{(1+k)^2}\cdot u\cdot\frac{d^2}{D_{\mathrm{m}}} \qquad (4)$$

The dashed lines in Fig. 7a–b are calculated on the basis of this theoretical expression. The full lines in Fig. 7a–b correspond to the total theoretical plate height $H_{\mathrm{tot,theo}}$ including the effect of the width w of the injection band:

$$H_{\mathrm{tot,theo}} = H_{\mathrm{col,theo}} + \frac{w^2}{12}\frac{1}{L_{\mathrm{eff}}} \qquad (5)$$

From the large difference between the dashed and the full lines, it can readily be concluded that the observed separation efficiencies indeed are strongly limited by the injection band width. For ultra-short

column experiments, such as the ones currently presented, this is however quasi inevitable (see, e.g., Refs. [6,18]). To obtain H values coming near the theoretical $H_{col,theo}$ values, the passage of the peaks should be recorded at positions much further downstream in our channels (around say $L=10$ mm or beyond). With the current set-up, this is momentarily impossible. Current work is therefore underway to build a photomultiplier-based set-up, allowing to monitor the separations further downstream of the channel inlet. As can be denoted from Fig. 7b, the $H_{col,theo}$ values which can be obtained in the absence of injection band width limitation can be as small as about 0.2 μm when using mobile phase velocities of $u>1$ cm/s.

Fig. 7 also shows that the currently investigated range of mobile phase velocities is still sub-optimal, such that it should be possible to achieve even faster separations. For this purpose, the sampling frequency of the detection system needs to be increased considerably beyond that of the currently employed CCD system. This will also be resolved when switching to a PMT-based detection scheme.

The remaining difference between the experimental H_{exp} values (calculated according to Eq. (2)) and the theoretical $H_{tot,theo}$ values should most probably be attributed to deviations from the perfect flat-rectangular channel cross-section shape and to imperfections in the stationary phase coating. For the latter, we do not really dispose of an effective quality inspection method.

Future research efforts will focus on the development of the detection gutter system presented in Ref. [14]. This system is based on the use of a transversally placed flow-through channel acting as a light pipe and running across the entire channel width, and perfectly combining the advantages of the large channel width (offering large optical path length) and the unique sub-micron channel thickness (preventing the light to escape from the light pipe) to potentially yield UV–Vis absorption detection limits similar to those in conventional HPLC and with an affordable loss in theoretical plate number. Another point of attention will be the application of a thicker stationary phase. For this purpose, we will in a first instance resort to the porous silicon anodisation techniques originally developed for the micro-electronics industry and perfectly compatible with the open-channel format of the SDC channels [20].

5. Conclusions

With a relatively simple set-up, we have been able to perform ultra-rapid reversed-phase LC separations in channels as thin as 100. In such channels, the separation kinetics are considerably enhanced with respect to the 5–10-μm channels typically used in open-channel CEC. The present demonstration of sub-0.1-s separations of a coumarin C440–460 mixture is a first indication of this fact. Since the presented data relate to ultra-short column separations, the obtained efficiencies are to a great extent reduced by the injection band width.

Before the SDC system can become a practical research tool, a huge leap in detection sensitivity and retention capacity however still needs to be made.

6. Nomenclature

C	tracer concentration dchannel thickness (m)
d	channel thickness (m)
D_{mol}	molecular diffusion coefficient (m^2/s)
H	height of equivalent theoretical plate (m)
k	retention factor (–)
N	theoretical plate number (–)
t	time coordinate (s)
u	mean mobile phase velocity (m/s)
u_{wall}	velocity of moving wall (m/s)
w	axial width of injected sample plug (m)
x	axial coordinate (m)

Greek symbol

σ_x^2	peak variance in the space domain (m^2)

Subscripts

col	column
eff	effective
exp	experimental

inj injection
theo theoretical

Acknowledgements

The authors greatly acknowledge the financial support from the Fonds voor Wetenschappelijk Onderzoek (FWO, grant no. KN 81/00), the University Research Council (grant nos. OZR 746 and OZR 597) and the Instituut voor Wetenschap en technologie (IWT, grant no. GBOU/010052). D.C. is supported through a specialization grant from the IWT (grant no. SB/1279/00).

References

[1] A. Manz, D.J. Harrison, E. Verpoorte, J.C. Fettinger, A. Paulus, H. Lüdi, H.M. Widmer, Adv. Chromatogr. 33 (1993) 1.
[2] D.J. Harrison, K. Fluri, K. Seiler, Z. Fan, C.S. Effenhauser, A. Manz, Science 261 (1993) 895.
[3] Y. Fintschenko, A. van den Berg, J. Chromatogr. A 819 (1998) 3.
[4] A.W. Moore, J.W. Jorgenson, Anal. Chem. 65 (1993) 3550.
[5] S.C. Jacobson, R. Hergenroder, L.B. Koutny, R.J. Warmack, J.M. Ramsey, Anal. Chem. 66 (1994) 1107.
[6] J.P. Kütter, S.C. Jacobson, N. Matsubara, J.M. Ramsey, Anal. Chem. 70 (1998) 3291.
[7] C.T. Culbertson, S.C. Jacobson, J.M. Ramsey, Anal. Chem. 72 (2000) 5814.
[8] R. Dadoo, R.N. Zare, C. Yan, D.S. Anex, Anal. Chem. 70 (1998) 4787.
[9] S.C. Jacobson, C.T. Culbertson, J.E. Daler, J.M. Ramsey, Anal. Chem. 70 (1998) 3476.
[10] W. Kok, Chromatographia (Suppl.) 51 (2000) S28.
[11] G. Desmet, G.V. Baron, J. Chromatogr. A 855 (1999) 57.
[12] G. Desmet, G.V. Baron, Anal. Chem. 72 (2000) 2160.
[13] H. Poppe, J. Chromatogr. A 778 (1997) 3.
[14] G. Desmet, N. Vervoort, D. Clicq, P. Gzil, A. Huau, G.V. Baron, J. Chromatogr. A 948 (2002) 19.
[15] G. Desmet, N. Vervoort, D. Clicq, G.V. Baron, J. Chromatogr. A 924 (2001) 111.
[16] N. Gottschlich, S.C. Jacobson, C.T. Culbertson, J.M. Ramsey, Anal. Chem. 73 (2001) 2669.
[17] A.P. O'Neill, P. O'Brien, J. Alderman, D. Hoffman, M. McEnery, J. Murrihy, J. Chromatogr. A 924 (2001) 259.
[18] L. Bousse, B. Dubrow, K. Ulfedler, in: A. van den Berg, J.D. Harisson (Eds.), Micro Total Analysis Systems 98, Kluwer, Dordrecht, 1998, p. 271.
[19] T.K. Sherwood, R.L. Pigford, C.R. Wilke, in: Mass Transfer, McGraw-Hill, New York, 1975.
[20] R.W. Tjerkstra, M. De Boer, E. Berenschot, J.G.E. Gardeniers, A. van den Berg, M.C. Elwenspoek, Electrochim. Acta 42 (1997) 3399.